Comparative Study of PLA Nanocomposites Reinforced with Clay and Silica Nanofillers and Their Mixtures

Evagelia Kontou, Michael Niaounakis, Panayiotis Georgiopoulos

Department of Applied Mathematical and Physical Sciences, Section of Mechanics, National Technical University of Athens, Athens, GR-15773, Greece

Received 29 October 2010; accepted 28 January 2011
DOI 10.1002/app.34234
Published online 26 May 2011 in Wiley Online Library (wileyonlinelibrary.com).

ABSTRACT: This study compares the effects of two different types of nanosized fillers (silica and montmorillonite) at three different weight fractions as well their mixtures on the thermomechanical properties of polylactide (PLA). The role of aggregation and interphase was investigated in terms of several experimental techniques, including scanning electron microscopy, wide-angle X-ray scattering (WAXS), thermogravimetric analysis, differential scanning calorimetry, dynamic mechanical analysis (DMA), and tensile measurements. The experimental results clearly suggest that silica and montmorillonite have different reinforcing and toughening effects on PLA, while the combination of the two different nanofillers has a detrimental effect on the tensile properties of the material. Four micromechanics models describing the Young's modulus of the nanocomposites were used to study the different matrix–nanofiller interactions. The best fit of the experimental results was obtained with a model that assumes the presence of an interphase surrounding each nanoparticle. The increase of the nanofiller content above a certain amount was not accompanied by a corresponding increase of the interphase, because the total nanofiller surface area was counterbalanced by the creation of aggregates. It is postulated that the aggregation effect acts antagonistically to the interphase effect. © 2011 Wiley Periodicals, Inc. J Appl Polym Sci 122: 1519–1529, 2011

Key words: nanocomposites; interfaces; biodegradable; polylactide; aggregates

INTRODUCTION

Poly(lactide) (PLA) is a thermoplastic material belonging to the family of environmental-friendly biodegradable polymers that has attracted a lot of attention in recent years.[1–3] PLA is used as a biocompatible polymer for applications in implants, surgical sutures, and controlled drug delivery systems, and it has also a great potential for applications in agriculture and in the packaging and catering industry.[4] However, its poor thermal and mechanical resistance and its limited barrier properties limit its access to those industrial sectors where biodegradability is required. One way to overcome these drawbacks is the addition of a small amount of nanosized fillers (2–5% by weight), which enhance the thermomechanical and barrier properties of pristine PLA.[5–7]

The polymer nanocomposites did not live up to the expectations as they did not provide substantial improvements to the properties of materials in comparison to the conventional microcomposites, although substantial savings to the costs and the weight of the materials can be achieved; for instance, it has been estimated that a nanocomposite with a nanofiller content of 4% by weight provides equivalent mechanical properties compared with a conventional microcomposite with a microfiller content of 20% by weight.[8,9] The main reason the mechanical properties of polymer nanocomposites still fall short of their theoretically predicted values is the inherent tendency of the nanoparticles to aggregate. The challenge in polymer nanocomposites is to obtain uniform and stable dispersion of nanofiller in the polymer matrix.

Several works have been focused on the preparation and study of biodegradable polymer-based nanocomposites.[10–13] A variety of nanofillers dispersion methods, such as *in situ* polymerization,[10,13] solution intercalation method in *N*-dimethylacetamide,[11] and melt intercalation technique using modified montmorillonite,[10,14] have been applied. Biodegradable nanocomposites were prepared[12] based on PLA and MMT with stacked intercalated and partially exfoliated morphologies.

So far, most of the nanocomposites reported in the literature are reinforced by one type of nanofiller. Combination of two different nanofillers has been reported for the reinforcement of polyacrylonitrile[15] and polypropylene.[16] The incorporation of Na-montmorillonite and silica into the polyacrylonitrile gave nanocomposites with highly enhanced thermal stabilities and mechanical properties compared with nanocomposites reinforced with either Na-montmorillonite or silica nanoparticles.[15] Similarly, the

Correspondence to: E. Kontou (ekontou@central.ntua.gr).

incorporation of nanosized $CaCO_3$ into PP/montmorillonite nanocomposites improved the mechanical properties of the nanocomposites.[16] The combination of two nanoparticles of different shapes apparently had a synergistic effect on the reinforcement of the matrix. On the other hand, the concurrent use of ZnO and Al_2O_3 nanofillers had a negative effect on the photostabilization of linear, low-density polyethylene.[17]

The aim of this article is to study the effect of two different types of nanosized fillers at three different weight fractions as well their mixtures on the thermomechanical properties of PLA. Silica nanoparticles, a commercial modified montmorillonite, and their mixture were used for the preparation of three series of nanocomposites. The majority of previous works has been dealt with layered silicates-based nanocomposites,[8,18–21] while in this work, a comparative study of the thermomechanical properties between the two nanofiller types and their mixture was made to detect the different matrix–filler interactions, occurring between PLA and either silica or montmorillonite nanoparticles. The experimental study of the thermomechanical properties was supplemented with a theoretical study involving the application of four micromechanics models, describing the Young's modulus of the three series of nanocomposites for the interpretation of the matrix–nanofiller interactions.

MATERIALS

PLA was supplied by NatureWorks LLC (Minnetonka, MN). The selected grade 2002D has a D content of 4.25%, a residual monomer content of 0.3%, and a density of 1.24 g/cm^3. The material in pellets form was dried at 45°C for a minimum of 8 h prior to use in a desiccating dryer.

Two different types of nanofillers and their mixtures were introduced in pristine PLA. Silica Aerosil R972 (supplied by Degussa Chemicals) (Marl, Germany) is hydrophobic fumed silica after treated with dimethyldichlorosilane and based on a hydrophilic fumed silica with a specific surface area of 130 m^2/g. The average primary size is 16 nm. Montmorillonite clay is of type Nanomer I30 E by Nanocor (Arlington Heights, Il) modified by octadecylamine.

EXPERIMENTAL

On the basis of PLA and the two nanofiller types, three series of PLA nanocomposites were prepared by melt mixing. The first two series, PLA/Si and PLA/MMT, consisted of PLA nanocomposites with a filler content of 2, 3, and 5 wt % of silica (Si) and montmorillonite clay (MMT), respectively; the third series contained PLA nanocomposites with a filler content of 4 wt % and a MMT/Si ratio of 60/40 and 40/60. In Table I, the materials with the corresponding filler weight and volume fractions are presented.

TABLE I
Weight and Volume Fractions of the Three Series of PLA/Nanocomposites

Sample type	Weight content (%)	Volume content (%)
PLA/Si/2	2	1.25
PLA/Si/3	3	1.88
PLA/Si/5	5	3.10
PLA/MMT/2	2	1.26
PLA/MMT/3	3	1.90
PLA/MMT/5	5	3.20
PLA/MMT60/Si40	4	2.50
PLA/MMT40/Si60	4	2.50

Melt mixing of nanofillers with PLA matrix was performed with a Brabender mixer at a temperature of 160°C, while the rotation speed of the screws was 40 rpm. The temperature for melt mixing was kept as low as possible to minimize the effect of degradation. The material was compression molded at 130°C, using a thermopress and a special mold of 2-mm thickness. The material was then cooled slowly down at ambient temperature. For each composition, two samples were prepared in the same manner, which provided reproducible results.

Scanning electron microscopy (SEM) images were obtained by direct observation of the topography of the sample's surface with a FEI QUANTA 200 (Hillsboro, Or) scanning microscope operated at acceleration voltage of either 15 or 20 kV and equipped with an energy dispersive system. All the studied samples were coated with carbon black to avoid charging under the electron beam.

Wide-angle X-ray scattering (WAXS) were recorded at room temperature in the range 2–60° (2θ) (step size = 0.02° and scanning rate 2 s/step) by using filtered Cu K_α radiation ($\lambda = 1.54$ Å). The type of the device was D500 SIEMENS (Munich, Germany).

Thermogravimetric analysis (TGA) was performed by using a TGA Q500 V20.2 Build 27 instrument by TA Instruments (New Castle, De) in an inert atmosphere of nitrogen. In a typical experiment, ~ 10 mg of the material was placed in the sample pan, and the temperature was equilibrated at 25°C. The temperature was then increased to 600°C at a rate of 20°C/min.

Calorimetric measurements [differential scanning calorimetry (DSC)] were carried out using a Setaram (Caluire, France) DSC 141 instrument calibrated with an Indium standard. Each sample was heated at a constant heating rate of 10°C/min from 20 to 170°C, and the thermogram was recorded. After heating up to 170°C, the PLA samples were isothermally held for 2 min and subsequently cooled down to 0°C at a cooling rate of 20°C/min. A second heating scan at 10°C/min was also performed. Both thermograms of first and second heating run were recorded. The degree of crystallinity was calculated by considering

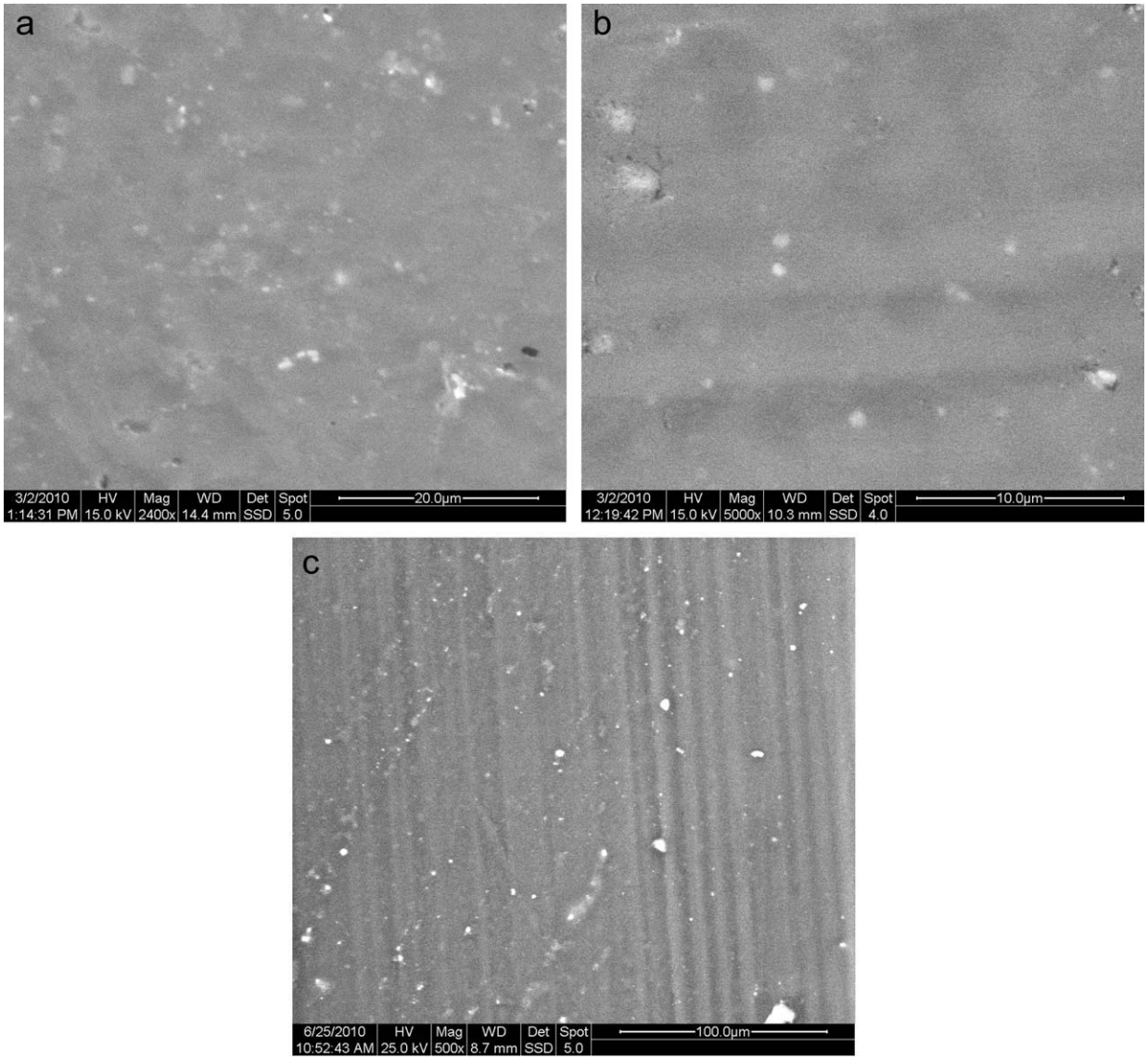

Figure 1 (a) SEM micrograph of PLA/Si/2 nanocomposite. (b) SEM micrograph of PLA/MMT/3 nanocomposite. (c) SEM micrograph of PLA/MMT40/Si60 nanocomposite.

a melting enthalpy of 93.1 J/g for 100% crystalline PLA.[22] DSC samples were taken from the center and the edge of a 2-mm thick PLA sheet, and it was found that the DSC results were repeatable, with an average scatter of lower than 5%.

Dynamic mechanical analysis (DMA) experiments were performed using the Perkin–Elmer (Norwalk, CT) DMA 7e instrument. The mode of deformation applied was the three-point bending system, and the mean dimensions of sample plaques were 2 mm $\times$ 4 mm $\times$ 20 mm. The temperature range varied from -50°C to 130°C. The temperature-dependent behavior was studied by monitoring changes in force and phase angle, keeping the amplitude of oscillation constant. The experiments were performed at a constant frequency of 1 Hz, and the heating rate was 5°C/min. The storage and loss moduli curves versus temperature were plotted.

Tensile measurements were performed with an Instron 1121 (Buckinghamshire, UK) type tester at room temperature. The dumbbell-type specimens were of a gauge length of 20 mm, and the applied crosshead speed was 0.5 mm/min. This value corresponds to an effective strain rate of 4.17×10^{-4} s^{-1}. The deformation could be measured very accurately with an experimental procedure that is based on a noncontact method with a laser extensometer, which is described in detail in a previous work.[23] Five specimens were tested for pristine PLA and each nanocomposite procedure, and the average scatter between experimental data was lower than 8%.

RESULTS AND DISCUSSION

Scanning electron microscopy

Representative SEM micrographs of PLA nanocomposites [Fig. 1(a–c)] reveal that both nanofiller types

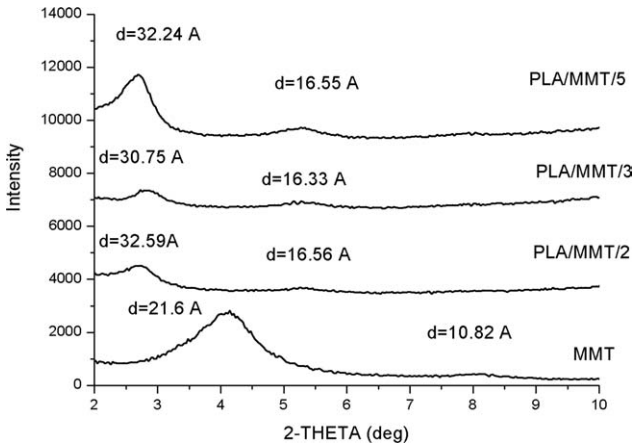

Figure 2 WAXS patterns of MMT and PLA/MMT nanocomposites at 2, 3, and 5 wt %.

examined have inherently the tendency for aggregate formation.[24] Namely, Figure 1(a–c) correspond to the micrographs of PLA/Si/5, PLA/MMT/2, and PLA/MMT40/Si60, respectively. It was found that PLA/Si/2 materials appear to have a homogenous distribution, and the average size of particles was varied from 150 to 300 nm. For PLA/Si/3, the particle distribution was not so homogeneous, with some particles being of the order of 200 nm, and larger agglomerates have also been observed. PLA/Si/5 materials are characterized by a distribution of agglomerates between 270 and 800 nm or greater. Analogous observations were made for PLA/MMT nanocomposites. PLA/MMT/2 appears to have smaller particles of an average size of 150 nm, coexisting with larger agglomerates of 300 or 600 nm. PLA/MMT/3 and PLA/MMT/5 are characterized by agglomerates of an average size of 600 and 900 nm, respectively. The PLA/Si/MMT nanocomposites are also characterized by the formation of aggregates with a larger average size compared with the other two series of PLA nanocomposites. More specifically, these materials show a more uniform dispersion of larger agglomerates, with an average size of 1200 nm, as shown in Figure 1(c).

Wide angle X-ray analysis

In Figure 2, the WAXS patterns of MMT and the corresponding PLA/MMT nanocomposites are presented for the range of 2θ between 2 and 10°. MMT is characterized by a single diffraction peak at $2\theta = 4.0°$ corresponding to the basal reflection, (001) accounting for a 21.6-Å interlayer distance. The shift of the clay diffraction peak to lower angles, as observed in Figure 2, corresponds to an increase of the interlayer distance of 11, 9.2, and 10.6 Å for 2, 3, and 5 wt % PLA/MMT nanocomposites, correspondingly, and indicates the creation of intercalated structures in the PLA/MMT nanocomposites. Although the gallery spacing of the clay platelets has been increased through the incorporation of PLA, there is still a high degree of layered order present in the clay tactoids. Two peaks at different interlayer distance are reported, suggesting the presence of different interlayer distances. The presence of the second-order peak usually suggests that a high degree of periodic order is present in the material.

Thermogravimetric analysis

Figures 3–5 show the TGA curves in terms of the percentage loss of weight versus temperature of pristine PLA and the three series of PLA/nanocomposites, respectively.

Table II summarizes the 10 wt % loss temperatures. The pristine polymer degrades without forming any residue, while the nanocomposites leave some residue, as it was expected. Compared with that of pristine PLA, the thermal stability of the three sets of PLA nanocomposites is increased. In particular, the 10 wt % loss temperature of all PLA nanocomposites, except of PLA/Si/2, is higher than that of PLA. The stabilities of the PLA/MMT/5 and PLA/Si/5 are higher than that of the pristine PLA by ~ 7 and ~ 4°C, respectively. The improved stability of the PLA/MMT/5 composite is attributed to the silicate layers acting as an insulating barrier. The PLA/MMT/Si nanocomposites have an intermediate thermal stability, close to that of PLA/MMT and PLA/Si materials, as shown in Figure 5.

The PLA decomposes almost completely (99%) at 387°C. The corresponding temperature shifts to higher values in all nanocomposites. The shifting is more pronounced for the PLA/MMT nanocomposites and reaches its maximum value with PLA/MMT/5. Furthermore, the thermal stabilities of the PLA/MMT nanocomposites are higher than those of

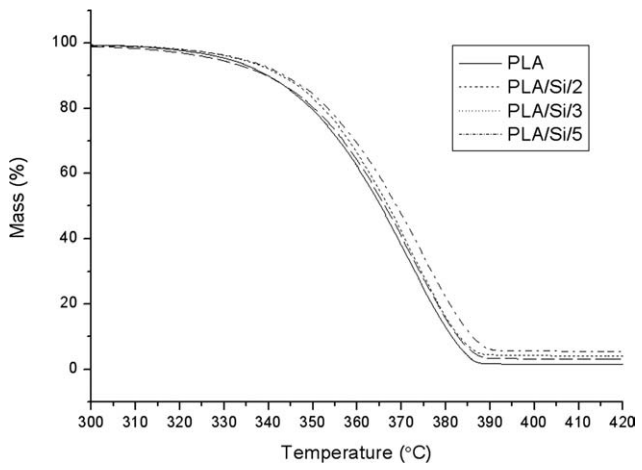

Figure 3 TGA mass loss curves of PLA/Si nanocomposites.

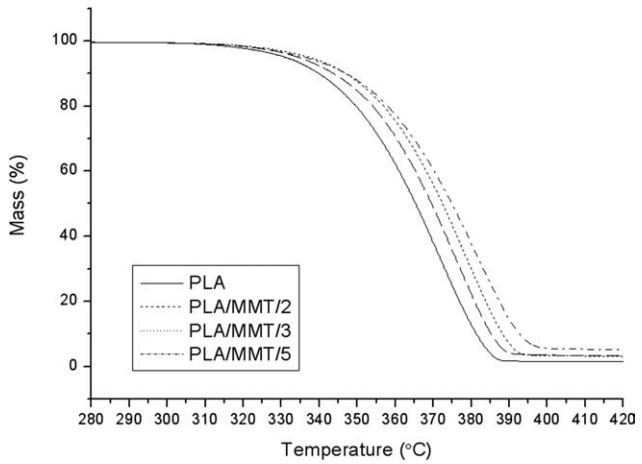

Figure 4 TGA mass loss curves of PLA/MMT nanocomposites.

the corresponding PLA/Si nanocomposites, while the terminal plateau value is also higher. It is concluded that the introduction of nanofillers increases the thermal stability of PLA, whereas the PLA/MMT materials seem to be more stable with respect to PLA/SiO_2 ones during the entire degradation process. As it is reported by Wu et al.[25] in PLA/clay nanocomposites, the increase in the thermal stability can be attributed to an ablative reassembling of the silicate layers, creating a physical protective barrier on the surface of the material. On the other hand, the delay of volatilization might be due to the labyrinth effect of the silicate layers dispersed in the nanocomposites.[26]

Generally, the introduction of inorganic components into organic materials can improve their thermal stability.[25]

Differential scanning calorimetry

The DSC thermograms are shown in Figures 6 and 7 for all material types tested. In Table III, the glass transition temperature and the melting measurements are summarized. Referring to the results of the second heating run, no endothermic or exothermic peak was detected. This behavior is in agreement with the reported slow crystallization rate of high molecular weight PLA, which does not allow the development of crystalline domains upon cooling.[27,28]

TABLE II
TGA 10 wt % Loss Temperature at a Rate of 20°C/min Under Nitrogen of PLA and PLA/Nanocomposites

Sample type	$T_{10\ wt\ \%}$ (°C)
PLA	340
PLA/Si/2	340
PLA/Si/3	343
PLA/Si/5	344
PLA/MMT/2	344
PLA/MMT/3	347
PLA/MMT/5	347
PLA/MMT40/Si60	344
PLA/MMT60/Si40	344

From the DSC experimental results of Table III, it is observed that the T_g of the PLA/Si and PLA/MMT nanocomposites is reduced with respect to the T_g of the pristine PLA material. In both series of nanocomposites, the nanofiller content variation does not affect the T_g values of the nanocomposites examined. In the PLA/MMT/Si nanocomposites, the T_g is close to the T_g of the pristine PLA material.

The T_g reduction, observed in the PLA/Si and PLA/MMT nanocomposites, is attributed to the increment of polymer mobility.[29,30] In such a case, the interphase between matrix and nanofillers must be poor because of the lack of connecting polymer from the nanoparticles to the surrounding polymer matrix.

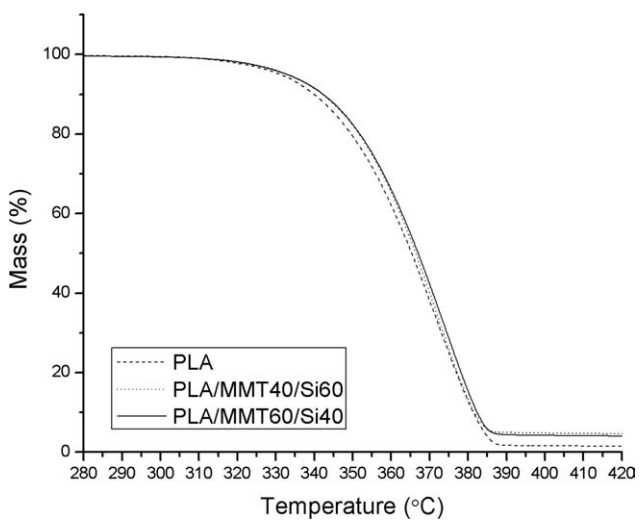

Figure 5 TGA mass loss curves of PLA/MMT/Si nanocomposites.

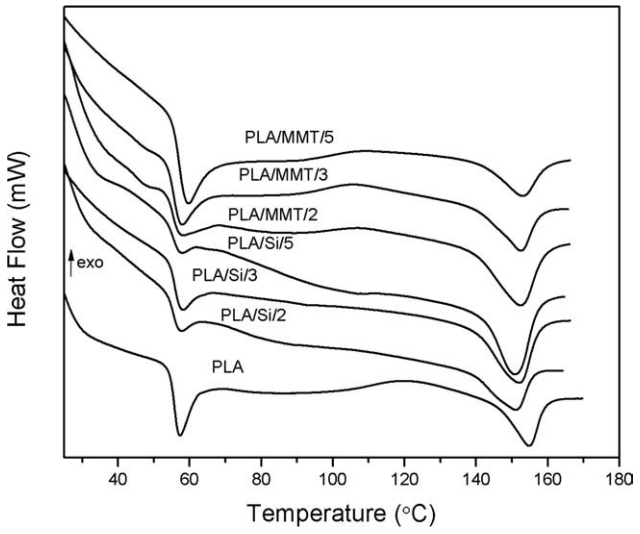

Figure 6 DSC thermograms of PLA, PLA/Si, and PLA/MMT nanocomposites at 10°C/min.

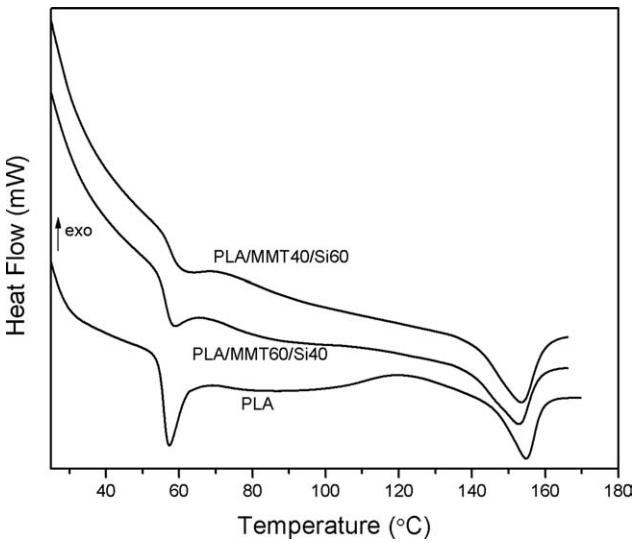

Figure 7 DSC thermograms at 10°C/min of PLA and PLA/MMT/Si nanocomposites.

The experimental fact that the T_g of the PLA/Si and PLA/MMT nanocomposites is not further affected by the nanofiller content is in contradiction with the established prior art opinion[31] that an increase of the nanofiller content is expected to diminish the interparticle distances and shift the T_g of the material to higher temperatures. A possible explanation to this discrepancy is the creation of aggregates in the matrix. The SEM images of the nanocomposites [see Fig. 1(a–c)] display large aggregates, and the size of the aggregates increases with the nanofiller content. Because of the creation of aggregates, the increase of the nanofiller content does not lead necessarily to an extra increase of the total nanofiller surface area. The MMT nanoparticles have greater tendency to create aggregates than the silica nanospheres because of their larger surface area.

In Figure 6, the PLA sample shows a broad cold crystallization (exotherm) area around 110°C. When cold crystallization occurs, less perfect crystallites are formed, which melt during the DSC heating run. The PLA/Si nanocomposites do not display a cold crystallization area. The PLA/MMT nanocomposites exhibit a cold crystallization area shifted to lower temperatures, around 97°C, while the total cold crystallization area increases with the MMT content (see also Table III). The lowering of the cold crystallization temperature in respect to pristine PLA indicates that the incorporation of clay considerably promotes kinetics and extent of PLA crystallization on heating.[5] Apparently, the MMT nanofiller acts as an effective nucleating agent speeding up PLA crystallization. On the other hand, the PLA/MMT/Si nanocomposites do not display cold crystallization, and their thermal behavior is similar to pristine PLA (see Fig. 7).

Regarding the melting behavior, the PLA sample shows a melting point at about 155°C and a heat of fusion of 19.50 J/g. The incorporation of silica nanoparticles or MMT clays affects the melting point of the materials slightly but leads to a substantial increment of heat of fusion, and subsequent increment of crystallinity content, as shown in Table III. This means that both nanofiller types act as nucleating agents, with the silica nanoparticles leading to relatively higher crystallinity content. On the other hand, both the PLA/MMT/Si nanocomposites exhibit a lower crystallinity content compared with the other two series of PLA nanocomposites. This behavior is attributed to the creation of larger agglomerates and the reduction of the number of available nucleation sites.

Dynamic mechanical analysis

The dynamic mechanical experimental results of all types of PLA/nanocomposites studied are presented in Figures 8 and 9. These figures display the temperature dependence of storage modulus E' and loss modulus E'' at a fixed frequency of 1 Hz. A general increment of E' with increasing nanofiller content for each series of nanocomposites is observed, which becomes more pronounced as temperature increases above T_g.

Table IV presents the comparative values of E' of all PLA/nanocomposites at different temperature

TABLE III
DSC Results of PLA and PLA/Nanocomposites

Sample type	T_g (°C)	Heat of fusion ΔH_m (J/g)	Melting point T_m (°C)	Percent crystallinity	Cold crystn. (on heating) T_{cc} (°C)	Crystn. (on cooling) T_c (°C)
PLA	58.0	19.5	155.0	20.9	110.0	94.0
PLA/Si/2	52.9	30.7	153.0	33.0	–	110 (broad)
PLA/Si/3	52.9	30.3	153.5	32.5	–	slightly broad
PLA/Si/5	52.7	29.2	152.5	31.3	–	94.0
PLA/MMT/2	55.2	20.7	153.4	22.2	97.0	93, 121 (bimodal)
PLA/MMT/3	55.2	29.1	153.4	31.3	96.5	119.3
PLA/MMT/5	55.4	25.7	154.0	27.6	97.6	90.0
PLA/MMT40/Si60	57.5	17.7	152.8	19.0	–	99.3
PLA/MMT60/Si40	57.3	19.6	153.4	21.1	–	100–140 (broad)

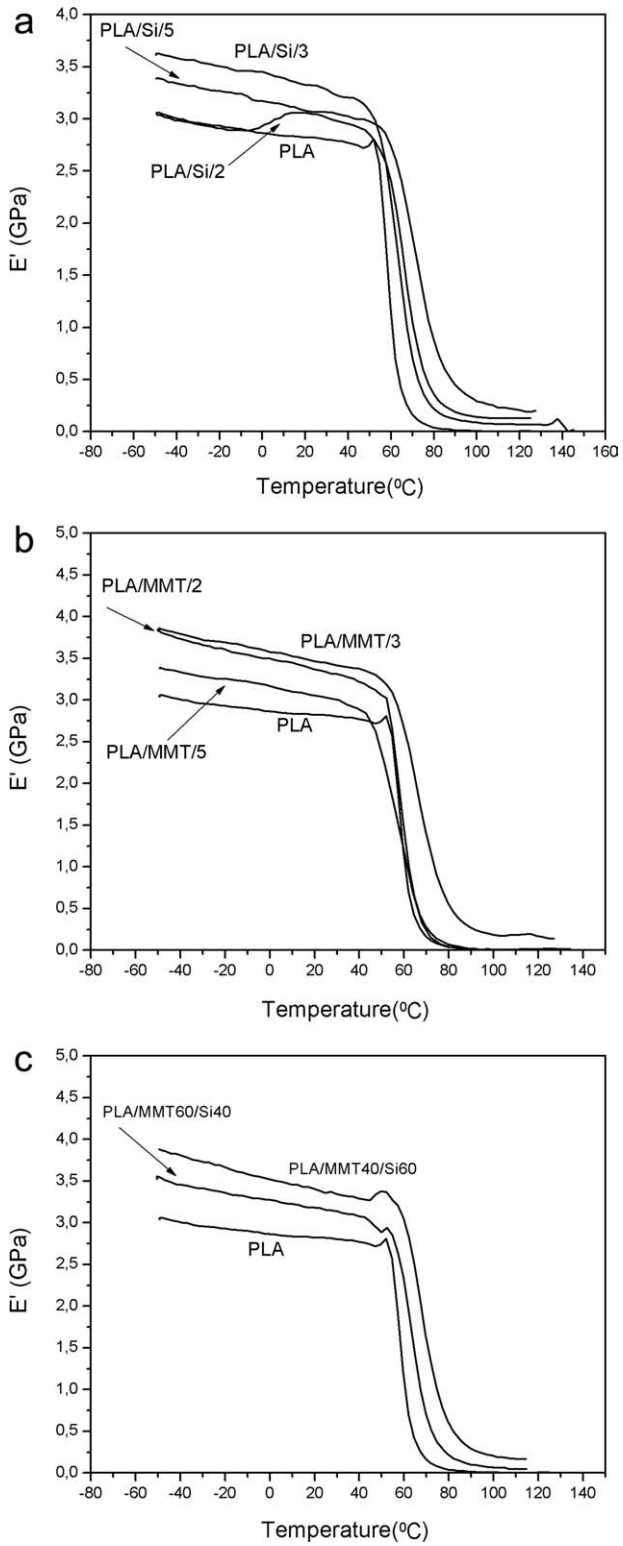

Figure 8 (a) Storage modulus versus temperature at 1 Hz of PLA and PLA/Si nanocomposites. (b) Storage modulus versus temperature at 1 Hz of PLA and PLA/MMT nanocomposites. (c) Storage modulus versus temperature at 1 Hz of PLA and PLA/MMT/Si nanocomposites.

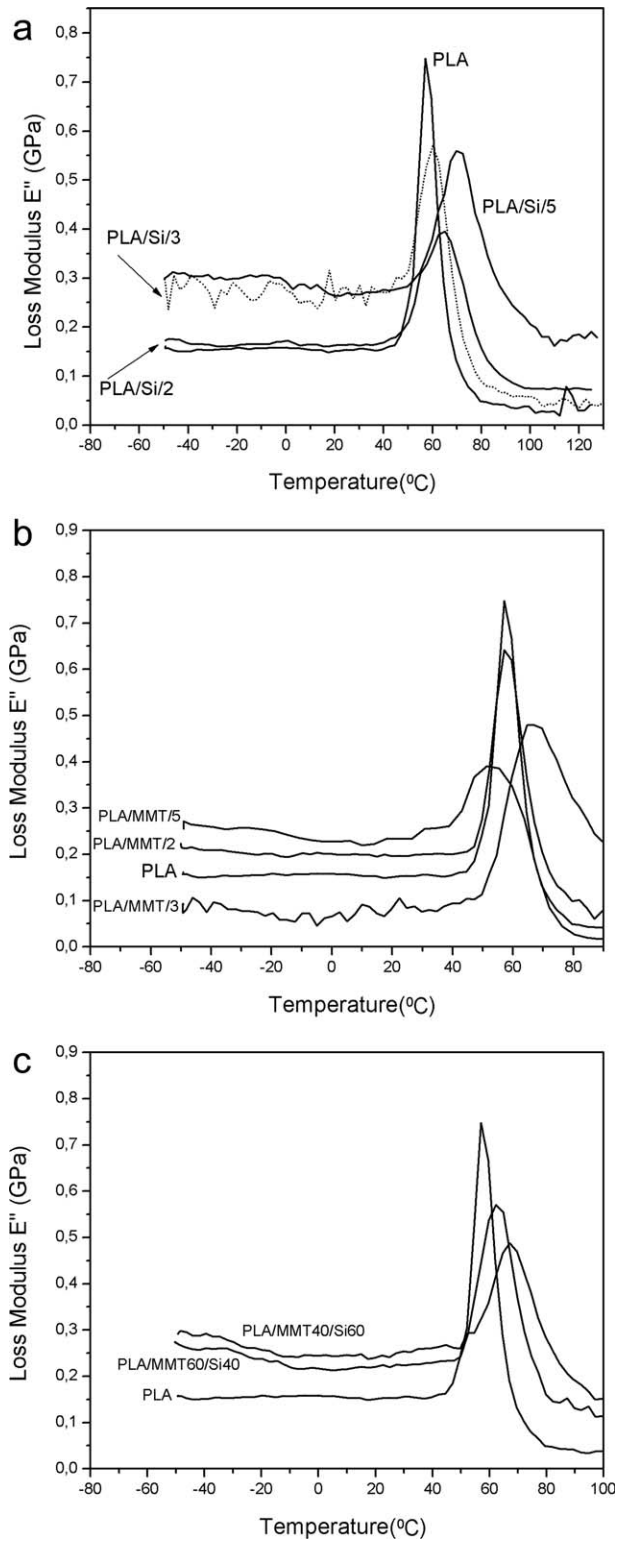

Figure 9 (a) Loss modulus versus temperature at 1 Hz of PLA/Si nanocomposites. (b) Loss modulus versus temperature at 1 Hz of PLA/MMT nanocomposites. (c) Loss modulus versus temperature at 1 Hz of PLA/MMT/Si nanocomposites.

ranges. As it can be seen, in the glassy state and the transition region, the PLA/MMT nanocomposites exhibit higher values of storage modulus enhancement in respect to the PLA/Si nanocomposites. In particular, at −30°C, increments of the order of 23.3, 26, and 11% are obtained for PLA/MMT/2, PLA/

TABLE IV
Storage Modulus Values of PLA and PLA/Nanocomposites at Various Temperature Ranges

Sample type	E' at −30°C (MPa)	E' at 30°C (MPa)	E' at 50°C (MPa)	E' at 65°C (MPa)	E' at 70°C (MPa)
PLA	2960	2800	2740	421	170
PLA/Si/2	2960	2960	2890	1760	1040
PLA/Si/3	3540	3280	3070	1360	988
PLA/Si/5	3300	3070	2980	2400	1880
PLA/MMT/2	3650	3320	3060	639	200
PLA/MMT/3	3720	3410	3250	2100	1430
PLA/MMT/5	3290	3000	2200	420	170
PLA/MMT60/Si40	3410	3140	2880	1420	704
PLA/MMT40/Si60	3730	3350	3380	2500	1660

MMT/3, and PLA/MMT/5, respectively. The corresponding values for PLA/Si/3 and PLA/Si/5 are 19% and 11.5%, respectively, while the PLA/Si/2 has the same modulus with the PLA matrix. This effect seems to be reversed above T_g (at about 70°C) where the PLA/Si nanocomposites appear to have much higher E' values. Regarding the nanocomposites with a nanofiller content of 5 wt %, the same reinforcement effect is obtained for both nanofiller types, in the glassy state, while at higher temperatures, the E' values of PLA/Si/5 are essentially higher than those of PLA/MMT/5.

Both PLA/MMT60/Si40 and PLA/MMT40/Si60 nanocomposites show a storage modulus increment of the order of 12 and 19.6%, respectively, at −30°C. At higher temperatures, PLA/MMT40/Si60 has the highest storage modulus values of all the PLA nanocomposites studied, as can be seen in Figure 8(c) and Table IV.

From Figure 8(a–c) and Table IV, it is deduced that for both nanofiller types, the highest thermomechanical enhancement in the glassy state is obtained at 3 wt %. At a higher nanofiller content, the reinforcement effect is reversed. This result means that the combination of an essential amount of nanofiller with a good quality dispersion can lead to better mechanical properties. At 5 wt %, the material is characterized by a large number of agglomerates, and it behaves as a conventional nanocomposite.

Regarding loss modulus data [Fig. 9(a–c)], no systematic dependence of the max E'' temperature was detected.

Tensile testing

The tensile results of pristine PLA and PLA nanocomposites are presented in Figures 10–12 and summarized in Table V. Regarding the PLA/Si nancomposites, shown in Figure 10, the highest modulus is obtained at a silica content of 2 wt % (37.4% increment), while the ductility is retained close to that of the pure matrix. The PLA/MMT nanocomposites, shown in Figure 11, exhibit a somehow different behavior. The highest modulus reinforcement occurs at 3 wt % (32.6% increment), while the PLA/MMT nanocomposites seem to be more brittle than the PLA matrix. Taking into account that the Young's modulus in a semicrystalline material depends on the crystallinity content, the earlier results are in consistency with the DSC data, where the two specific nanocomposites with the highest modulus appear to a have a maximum crystallinity content of 33 and 31.3%, respectively.

The modulus of the PLA/Si nanocomposites changes slightly with the silica content, while the modulus of the PLA/MMT nanocomposite increases with the MMT content. WAXS and SEM revealed the presence of intercalated and aggregated structures in the PLA/MMT nanocomposites. At MMT contents of 3 and 5 wt %, the nanocomposites become more brittle, and the tensile strength drops apparently because of the formation of agglomerates.

As can be seen in Figures 10–12 and Table V, the yield strain of all PLA nanocomposites is lower than the one of pristine PLA.

With regard to PLA/MMT/Si nancomposites, both samples exhibit the same modulus, which is

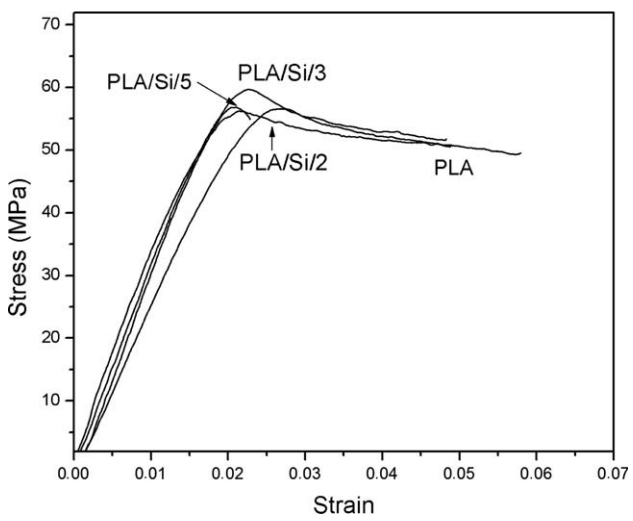

Figure 10 Tensile stress–strain curves at a rate of 4.17 10^{-4} s^{-1} of PLA and PLA/Si nanocomposites.

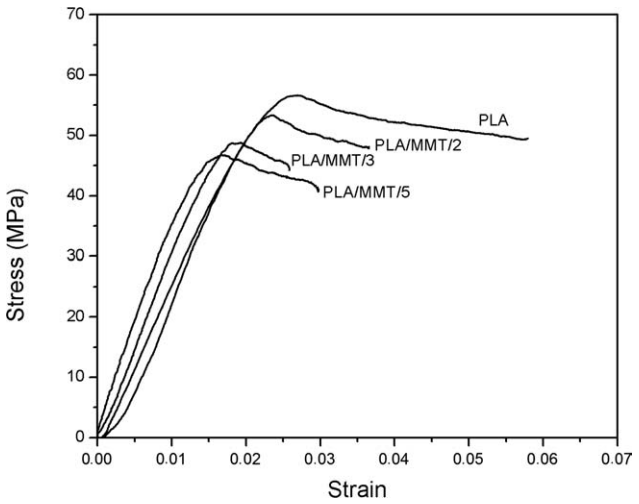

Figure 11 Tensile stress–strain curves at a rate of 4.17 10^{-4} s^{-1} of PLA and PLA/MMT nanocomposites.

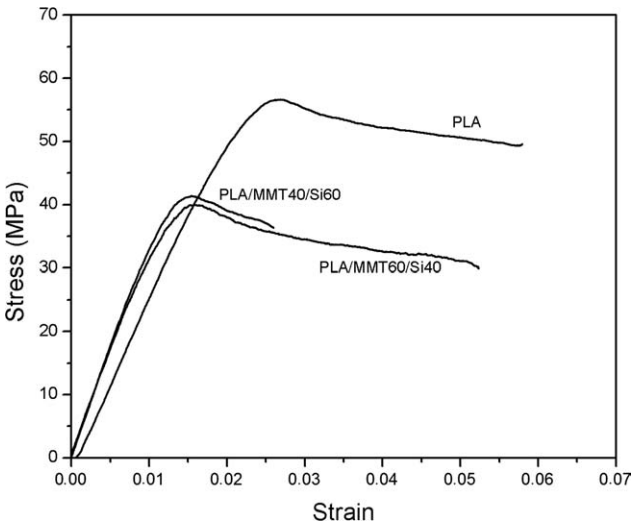

Figure 12 Tensile stress–strain curves at a rate of 4.17 10^{-4} s^{-1} of PLA and PLA/MMT/Si nanocomposites.

higher than the modulus of pristine PLA, as is shown in Figure 12 and Table V. Furthermore, the yield stress and yield strain of the PLA/MMT/Si nanocomposites are substantially lower than the yield stress and yield strain of pristine PLA and of all the PLA/Si and PLA/MMT nanocomposites. The decrease of yield stress is attributed to the debonding of the nanofillers from the matrix. In a system where the interfacial adhesion is not high, debonding could occur at a lower tensile stress than the yield stress of pristine PLA.[19,32] This peculiar behavior can be explained as follows.

The decrement of yield stress and the increment of the initial slope of the stress–strain curve is not typical in conventional particulate composites, where yield stress is enhanced because of the filler's presence. As it was reported in a previous work,[33] the yield behavior of polymeric structure is affected mainly by two factors, namely the accumulated strain (in respect to the imposed strain rate) and the distributed nature of various defects onto the polymeric bulk. Given that a number of free volume holes and/or other type defects are distributed into the matrix, the imposed strain will be preferably installed in these regions, and therefore, a distribution of strain is established into the material. Hereafter, the onset of yielding will be emerged at these localized regions, with extra free volume or density fluctuations. The presence of a nanoparticle will lead to a perturbation of polymeric bulk around it, and as it has been reported elsewhere,[34] it is a matter of interest whether this effect is directly responsible for the mechanical behavior of the materials. The presence of nanofillers, and especially the mixture of the two nanofiller types, seems to cause the development of additional localized regions with different size and extent compared with those developed in the two other series of PLA/nanocomposites. This inhomogeneity leads to the emergence of yielding at a lower macroscopic strain, resulting to a higher modulus but to a lower yield stress. This effect seems to be more intense in PLA/MMT/Si nanocomposites, where the formation of larger and different type agglomerates possibly leads to the creation of larger holes causing the agglomerates to debond from the matrix, and since the debonded nanoparticles do not transfer any external load, the yield stress decreases.

TABLE V
Tensile Results of PLA and PLA/Nanocomposites

Sample type	Young modulus (MPa)	Yield stress (MPa)	Yield strain	Tensile strength (MPa)	Strain at break
PLA	2800	56.0	0.026	47.8	0.056
PLA/Si/ 2	3846 (37.4%)	57.0	0.021	51.8	0.050
PLA/Si/ 3	3300 (17.9%)	61.0	0.023	53.0	0.048
PLA/Si /5	3436 (22.7%)	57.0	0.021	55.0	0.023
PLA/MMT/2	3200 (14.3%)	54.0	0.024	51.0	0.037
PLA/MMT/3	3713 (32.6%)	49.0	0.018	48.0	0.027
PLA/MMT/5	3650 (30.4%)	47.0	0.016	48.0	0.030
PLA/MMT60/Si40	3300 (17.8%)	40.0	0.015	32.0	0.052
PLA/MMT40/Si60	3323 (18.7%)	42.0	0.015	39.0	0.026

TABLE VI
Experimental Data of Relative Young's Modulus and the Corresponding Theoretical Values Predicted by Four Well-Known Micromechanics Models

Sample type	E_c/E_m (experimental)	Mori–Tanaka model	Chen model	Taya–Chou model	Odegard model	Young's modulus (MPa)
PLA	1.00	–	–	–	–	2800
PLA/Si/ 2	1.37	1.02	1.02	1.02	1.36	3846
PLA/Si/ 3	1.18	1.03	1.03	1.03	1.18	3300
PLA/Si /5	1.23	1.06	1.06	1.05	1.20	3436
PLA/MMT/2	1.14	1.02	1.02	1.02	1.17	3200
PLA/MMT/3	1.33	1.03	1.03	1.03	1.33	3713
PLA/MMT/5	1.30	1.06	1.06	1.05	1.31	3650
PLA/MMT60/Si40	1.18	1.04	1.04	1.04	1.18	3300
PLA/MMT40/Si60	1.18	1.04	1.04	1.04	1.18	3323

Modeling

Table VI compares the experimental values of relative Young's modulus, i.e., the composite's modulus over the modulus of PLA matrix (E_c/E_m), of the various studied material types with the corresponding theoretical values predicted by four well-known micromechanics models of Mori–Tanaka, Chen, Taya–Chou, and Odegard.[35–38] From these results, it becomes apparent that the first three models, which were designed for conventional composite materials, are not able to describe adequately the reinforcement induced by the nanofillers because of the very low filler content (up to 5 wt %). On other hand, the Odegard's model, which takes into account the so-called "interphase," i.e., the specific region developed around nanoparticles, describes satisfactorily the reinforcement effect. In all material types, the interphase modulus, E_i was fitted to be equal to 7 GPa. The calculated interphase volume values were 0.55 for the PLA/Si/2 nanomposite and 0.2 for both PLA/Si/3 and PLA/Si/5 nanocomposites. A different trend was found for PLA/MMT nanocomposites, namely 0.2 for PLA/MMT/2, 0.45 for PLA/MMT/3, and 0.4 for PLA/MMT/3. The interphase volume fraction of the PLA/MMT/Si nanocomposites was 0.18. The reduced total interphase volume of both samples is in agreement with the corresponding tensile results, meaning that the combination of the two different nanofillers has a detrimental effect on the properties of the material. The decrease of the interphase volume might be due to the formation of large agglomerates.

Although the Odegard's model presents the best fitting in comparison with the other tested models, it still deviates from the experimental data. This deviation could be attributed to the presence of a (multimodal) particle size distribution as a result of the formation of aggregates in the polymer matrix, the effect of which has not been taken into account.

On the basis of the experimental and theoretical results, it is postulated that the aggregation effect acts antagonistically to the interphase effect. The increase of the nanofiller content above a certain amount is not accompanied by a corresponding increase of the interphase, because the total nanofiller surface area is counterbalanced by the creation of aggregates which compromise the expected properties improvement.

CONCLUSIONS

In this article, a comparative study of the thermomechanical properties between two nanofiller types of different shapes was made to detect the different matrix–filler interactions occurring between PLA and either silica or montmorillonite nanoparticles as well their mixtures.

With reference to the Young's modulus, the optimum nanofiller was 2 wt % and 3 wt % for silica and MMT, respectively. On the other hand, the PLA/Si nanocomposite with filler content of 3 wt % silica gave the highest yield stress.

Both nanofiller types acted as nucleating agents, leading to an increment of crystallinity content. On the other hand, the combination of the two nanofillers reduced the crystallinity of the material. Furthermore, the T_g of all PLA/nanocomposites is lower the T_g of pristine PLA.

The concurrent addition of two nanofillers caused the yield stress to decrease and the Young's modulus to increase compared with pristine PLA matrix. Theoretical calculations based on the Odegard's model showed that the PLA/MMT/Si nanocomposites have the smallest interphase volume fraction (0.18), and as a result, they are prone to debonding. In general, the mechanical properties of the PLA/MMT/Si nanocomposites were inferior than the nanocomposites reinforced with either MMT or silica nanoparticles. This behavior was attributed to the formation of large agglomerates.

The increase of the nanofiller content above a certain amount (>3 wt %) is not accompanied by a

corresponding increase of the interphase, because the total nanofiller surface area is counterbalanced by the creation of aggregates which compromise the expected properties improvement.

References

1. Södergård, A.; Stolt, M. Prog Polym Sci 2002, 27, 1123.
2. Pan, P.; Zhu, B.; Kai, W.; Dong, T.; Inoue, Y. J Appl Polym Sci 2007, 107, 54.
3. Yang, H.; Yoon, J.; Kim, M. Polym Degrad Stab 2005, 87, 131.
4. Hoshino, A.; Tsuji, M.; Ito, M.; Momochi, M.; Mizutani, A.; Takakuwa, K.; Higo, S.; Sawada, H.; Uematsu, S. In Biodegrable Polymers and Plastics; Chiellini, E., Solaro, R., Eds.; Springer US: New York, 2003; p47.
5. Fukushima, K.; Abbate, C.; Tabuani, D.; Gennari, M.; Camino, G. Polym Degrad Stab 2009, 94, 1646.
6. Ray, S. Prog Mater Sci 2005, 50, 962.
7. McNeill, I.; Leiper, H. Polym Degrad Stab 1985, 11, 309.
8. Thellen, C.; Orroth, C.; Froio, D.; Ziegler, D.; Lucciarini, J.; Farrell, R.; D'Souza, N.; Ratto, J. Polymer 2005, 46, 11716.
9. Zhou, Y.; Rangari, V.; Mahfuz, H.; Jeelani, S.; Mallick, P. Mater Sci Eng: A 2005, 402, 109.
10. Paul, M.; Alexandre, M.; Degee, P.; Henrist, C.; Rulmont, A.; Dubois, P. Polymer 2003, 44, 443.
11. Chang, J.; An, Y.; Sur, G. J Polym Sci Part B: Polym Phys 2002, 41, 94.
12. Feijoo, J.; Cabedo, L.; Gimenez, E.; Lagaron, J.; Saura, J. J Mater Sci 2005, 40, 1785.
13. Pantoustier, N.; Lepoittevin, B.; Alexandre, M.; Dubois, P.; Kubies, D.; Calberg, C.; Jérôme, R. Polym Eng Sci 1928, 2004, 42.
14. Lepoittevin, B.; Devalckenaere, M.; Pantoustier, N.; Alexandre, M.; Kubies, D.; Calberg, C.; Jérôme, R.; Dubois, P. Polymer 2002, 43, 4017.
15. Yu, T.; Lin, J.; Xu, J.; Chen, T.; Lin, S.; Tian, X. Compos Sci Technol 2007, 67, 3219.
16. Tang, Y.; Hu, Y.; Zhang, R.; Wang, Z.; Gui, Z.; Chen, Z.; Fan, W. Macromol Mater Eng 2004, 289, 191.
17. Yang, R.; Li, Y.; Yu, J. Polym Degrad Stab 2005, 88, 168.
18. McLauchlin, A. R.; Thomas, N. L. Polym Degrad Stab 2009, 94, 868.
19. Jiang, L.; Zhang, J.; Wolcott, M. Polymer 2007, 48, 7632.
20. Li, B.; Dong, F.; Wang, X.; Yang, J.; Wang, D.; Wang, Y. Eur Polym J 2009, 45, 2996.
21. Sinha Ray, S.; Yamada, K.; Okamoto, M.; Fujimoto, Y.; Ogami, A.; Ueda, K. Polymer 2003, 44, 6633.
22. Fischer, E. W.; Sterzel, H. J.; Wegner, G. Colloid Polym Sci 1973, 251, 980.
23. Kontou, E.; Farasoglou, P. J Mater Sci 1998, 33, 147.
24. Wu, C.; Zhang, M.; Rong, M.; Friedrich, K. Compos Sci Technol 2002, 62, 1327.
25. Wu, D.; Wu, L.; Zhang, M. Polym Degrad Stab 2006, 91, 3149.
26. Gilman, J.; Kashiwagi, T.; Giannelis, E.; Manias, E.; Lomakin, S.; Lichtenhan, J.; Jones, P. Spec Publ R Soc Chem 1998, 224, 203.
27. Tsuji, H.; Ikarashi, K.; Fukuda, N. Polym Degrad Stab 2004, 84, 515.
28. Signori, F.; Coltelli, M.-B.; Bronco, S. Polym Degrad Stab 2009, 94, 74.
29. Ash, B.; Siegel, R.; Schadler, L. J Polym Sci Part B: Polym Phys 2004, 42, 4371.
30. Zax, D.; Yang, D.; Santos, R.; Hegemann, H.; Giannelis, E.; Manias, E. J Chem Phys 2000, 112, 2945.
31. Becker, C.; Krug, H.; Schmidt, H. Mater Res Soc Symp Proc 1996, 435, 237.
32. Zuiderduin, W.; Westzaan, C.; Huetink, J.; Gaymans, R. Polymer 2003, 44, 261.
33. Spathis, G.; Kontou, E. Polymer 2008, 49, 4462.
34. Papakonstantopoulos, G.; Yoshimoto, K.; Doxastakis, M.; Nealey, P.; de Pablo, J. Phys Rev E 2005, 72, 31801.
35. Mori, T.; Tanaka, K. Acta Metall 1973, 21, 571.
36. Chen, C.; Cheng, C. Int J Solids Struct 1996, 33, 2519.
37. Taya, M.; Chou, T. Int J Solids Struct 1981, 17, 553.
38. Odegard, G. M.; Clancy, T. C.; Gates, T. S. Polymer 2005, 46, 553.